

First observation of reactor antineutrinos by coherent scattering

N. Ackermann¹, H. Bonet¹, A. Bonhomme^{1,a}, C. Buck¹,
K. Fülber², J. Hakenmüller^{1,b}, J. Hempfling¹, G. Heusser¹,
M. Lindner¹, W. Maneschg¹, K. Ni¹, M. Rank³, T. Rink^{1,c},
E. Sánchez García¹, I. Stalder³, H. Strecker¹, R. Wink²,
J. Woenckhaus^{3,d}

¹MPIK Heidelberg, Saupfercheckweg 1, 69117 Heidelberg, Germany.

²PreussenElektra GmbH, Kernkraftwerk Brokdorf, Osterende,
25576 Brokdorf, Germany.

³Kernkraftwerk Leibstadt AG, 5325 Leibstadt, Switzerland.

^a*Present address:* IPHC, CNRS, 67037 Strasbourg, France.

^b*Present address:* Duke University, Durham, NC 27708, USA.

^c*Present address:* KIT, Hermann-von-Helmholtz-Platz 1,
76344 Eggenstein-Leopoldshafen, Germany.

^d*Present address:* PSI, Forschungsstrasse 111, 5232 Villigen, Switzerland.

Abstract

Neutrinos are elementary particles that interact only very weakly with matter. Neutrino experiments are therefore usually big, with masses on the multi-ton scale. The thresholdless interaction of coherent elastic scattering of neutrinos on atomic nuclei leads to drastically enhanced interaction rates, that allows for much smaller detectors. The study of this process gives insights into physics beyond the Standard Model of particle physics. The CONUS+ experiment was designed to first detect elastic neutrino-nucleus scattering in the fully coherent regime with low-energy neutrinos produced in nuclear reactors. For this purpose, semiconductor detectors based on high-purity germanium crystals with extremely low energy threshold of 160–180 eV were developed. Here we show the first observation of a neutrino signal with a statistical significance of 3.7 sigma from the CONUS+ experiment, operated at the nuclear power plant in Leibstadt, Switzerland. In 119 days of reactor operation (395 ± 106) neutrinos were measured compared to a predicted number from calculations assuming standard model physics of (347 ± 59) events. The good agreement between data and prediction constrains

many parameters in various theoretical models. With increased precision, there is potential for fundamental discoveries in the future. The CONUS+ results in combination with other measurements of this interaction channel might therefore mark a starting point for a new era in neutrino physics.

Introduction

Neutrinos are known for their very tiny interaction rate with matter. This is why they are usually very hard to detect, despite their high abundance and the existence of very strong neutrino sources. The most common detection channels such as the inverse beta decay reaction or neutrino-electron scattering usually require target masses in the ton to kiloton scale. In the Standard Model (SM) of particle physics, neutrinos can couple to quarks by the exchange of a mediating Z boson. For small momentum exchanges, the possibility of coherent scattering of neutrinos on the sum of all nucleons of an atomic nucleus was predicted in 1974 [1]. For this interaction the reaction rate (cross-section) is enhanced by few orders of magnitude as it scales approximately with the squared number of neutrons in the target nucleus. Therefore, it is in principle possible to construct neutrino detectors on the kilogram scale using this channel.

Neutrino sources suitable for the measurement of the coherent elastic neutrino-nucleus scattering ($\text{CE}\nu\text{NS}$) need to have energies of a few up to tens of MeV. Intense neutrino sources fulfilling this condition are, for example, the Sun, supernova explosions, accelerator-based sources, or nuclear reactors. It took 43 years after its prediction until $\text{CE}\nu\text{NS}$ was first detected in 2017 by the COHERENT experiment in a scintillating crystal of cesium iodide [2]. Here, the neutrinos are generated at a Spallation Neutron Source (SNS) when pions decay at rest. At the same neutrino source the $\text{CE}\nu\text{NS}$ measurement was confirmed with argon [3] and germanium [4] as target materials. Nuclear reactors emit neutrinos of lower energies than SNS sources. This has the advantage of a strongly enhanced sensitivity for several parameters in beyond the standard model (BSM) theories. However, it makes the detection of neutrinos much harder because of the requirement of extremely low energy thresholds in the detector.

There is a long history of successful experiments using reactor antineutrinos as sources, including the first neutrino detection in 1956 [5]. An intense antineutrino flux is produced after the fission process during the beta decay of the fission fragments. Nuclear reactors can be considered as well-defined, pure and point-like sources of specific neutrino flavor type, the electron antineutrinos. In recent years, reactor experiments allowed to study neutrino oscillation parameters [6–9] and constrain the existence of sterile neutrinos [10–13]. Today, there is a worldwide effort to measure $\text{CE}\nu\text{NS}$ close to nuclear reactors [14–23]. In terms of neutrino oscillation studies, it is a complementary approach, since $\text{CE}\nu\text{NS}$ is sensitive to all known neutrino flavors, the electron, muon and tau neutrinos/antineutrinos, whereas the inverse beta decay as standard detection technique for reactor neutrinos is only sensitive to electron antineutrinos. In addition, there is a wide range of studies and topics that can be addressed in $\text{CE}\nu\text{NS}$ measurements. For example, they can be used to probe nuclear

structures, they are highly relevant in astrophysics, and they also provide important input for present and future dark matter experiments, which are limited in sensitivity by the $CE\nu NS$ rate of solar neutrinos. Very recently, first indications for such a $CE\nu NS$ signal were found in dark matter experiments with xenon as target [24, 25]. Moreover, CONUS+ technology has the potential to use neutrinos for reactor monitoring and safeguard applications in the future.

The CONUS and CONUS+ experiments

The CONUS experiment [18] began operating in 2018 at the nuclear power plant in Brokdorf, Germany (KBR). There, the experiment took data until 2022 at a distance of only 17.1 m from the center of the reactor core. At the maximum thermal power of the reactor of 3.9 GW, the corresponding flux at the detector position was estimated to be $2.3 \cdot 10^{13}$ antineutrinos per cm^2 and second. The experimental setup consisted of four high-purity germanium (HPGe) detectors. Each diode had a mass of about 1 kg leading to a total fiducial germanium mass of 3.73 ± 0.02 kg [26]. As a final result of the measurement at KBR, the neutrino flux was constrained with 90% confidence level to a factor 1.6 above the signal expectation [27]. This world-best upper limit on the $CE\nu NS$ interaction rate at nuclear reactors so far allowed us to exclude significant deviations from the SM or to test the standard description of signal quenching due to dissipation effects in the germanium material in the energy region of interest.

In 2023, the CONUS setup moved to another power plant in Leibstadt, Switzerland (KKL), since the reactor at KBR stopped operation. At KKL the experiment continued as CONUS+. Here, antineutrinos are created in a boiling water reactor with a thermal power of 3.6 GW. The setup is placed at a distance of about 20.7 m from the center of the KKL reactor core. Before installation, the HPGe detectors called C2–C5 were refurbished to improve the energy threshold and the detection efficiency at low energy. In this way, the sensitivity was improved despite a higher level of environmental radioactivity and a slightly lower nominal neutrino flux of $1.5 \cdot 10^{13}$ antineutrinos/ (cm^2s) at the new site. The predicted number of neutrino interactions in the four detectors increased almost an order of magnitude, mainly due to the improved energy threshold and trigger efficiency [28].

The search for $CE\nu NS$ in nuclear reactors is a challenging task for various reasons. Since a high neutrino flux is required, positions close to the reactor core inside the reactor building are preferred. The environment inside this inner control zone is quite different from the working conditions in a common research laboratory. There are several restrictions related to the materials allowed, earthquake safety, access, data transfer, etc. Appropriate solutions on all these topics were found in close cooperation with the KBR and KKL staff. In addition, there is limited protection against cosmic radiation, as the overburden at the CONUS+ site corresponds only to the equivalent 7.4 m water. In general, the radioactivity level has to be kept under control to perform successful rare event searches. For example, cosmic muons produce electromagnetic cascades and neutrons in the building structure and shield materials. These cascades can create event signatures similar to neutrinos in the HPGe detectors. Mitigation of detector signals created by such cosmic radiation or environmental radioactivity

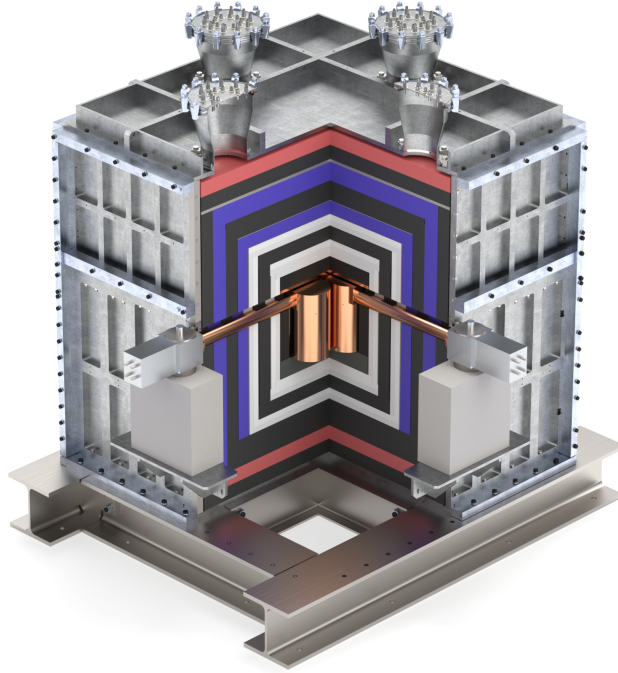


Fig. 1: The CONUS+ shield with a weight of about 10 tons is installed inside the reactor building of the nuclear power plant in Leibstadt. It is mechanically stabilized by a stainless steel (silver) frame to assure integrity of the setup in case of an earthquake. Layers of lead (black) reduce the impact from external gamma radiation, polyethylene (red) and boron-doped polyethylene (white) moderate and capture neutrons emitted from the reactor. Two layers of plastic scintillator plates are equipped with photo multipliers (blue) and are used as an active veto system discriminating background from cosmic muons. In the central detector chamber, four germanium diodes are operated inside radiopure copper cryostats and connected to electrically powered cryocoolers.

(background events) is achieved by using an effective shield structure around the detectors [28] as depicted in Fig.1. Furthermore, the energy of the nuclear recoils after neutrino scattering is very low. The unit used for the energy measured by the Ge detectors is given in eV ($1.6 \cdot 10^{-19}$ J) and should be interpreted as ionization energy. It was a longstanding effort to reach the required threshold levels in the detectors. Our currently lowest threshold level of 160 eV is only two orders of magnitude above the typical semiconductor band gap, which defines the minimum energy to create one electron-hole pair.

Neutrino signal observation in CONUS+

The basic concept of antineutrino detection in CONUS+ is to measure an energy spectrum under stable conditions in phases for which the reactor is running or stopped

(reactor on and off). Most events originate from cosmic radiation, which is fully independent of the reactor operation condition. During on-phases additional neutrino events on top of the cosmogenic background contribution are expected with a characteristic spectral shape. The neutrino signal can be extracted from a comparison of the data sets with the reactor on and off. The reactor off-phases without neutrino signal are obtained in maintenance periods for refueling, which are typically once per year with a duration of approximately 1 month.

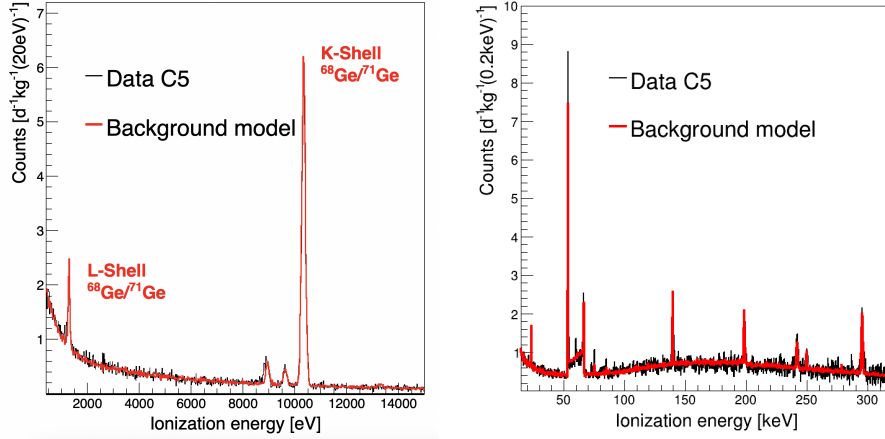


Fig. 2: The plot on the left shows the background spectrum directly above the energy range in which the neutrino signal is expected. The data (black line) is shown for the reactor on period and is based on the measurement of the detector with the lowest background in the CONUS+ analysis (C5). This data is compared to the background model (red line) and found to be in good agreement. The high energy channel up to few hundred keV is shown on the right.

The energy spectrum measured between [0.4 – 15] keV during reactor on period is depicted in Fig.2, together with the expected background calculated using a well-validated GEANT4 framework [29]. A good understanding of the background composition is mandatory for our neutrino analysis. Following the experience gained at the Brokdorf reactor, the background spectra were adjusted to the new site in Leibstadt. The contributions of muon-induced, neutron and gamma components were validated in a dedicated measurement campaign with multiple detector technologies before installing the CONUS+ setup [30]. Uncorrelated background contributions, which are independent of the reactor thermal power condition, are measured in the reactor off-phase.

The dominant background contributions, such as the muon-induced or neutron background, are identical for the three detectors used in the analysis. A comparison between background model and data is shown in Fig.2. In addition to the neutrons, which are created by muons in the materials of the CONUS+ shield, there is a relevant

fraction of direct neutrons up to 100 MeV energy already produced in the atmosphere in cosmic ray air showers. The background during reactor off was lower since a vessel lid with a thickness of a few cm of steel was placed right above the CONUS+ room during reactor outage providing additional overburden. According to simulations, this reduction was 3% for muons and 19% for direct cosmic neutrons. Other components contributing to the background spectrum are from metastable states in germanium and the radioactive noble gas radon. Variations in the radon level inside the detector chamber were corrected. Otherwise, no significant differences are observed during reactor on and off. The reactor correlated background events, in particular the ones from neutrons produced in the reactor, are thoroughly studied in [30] and found to be negligible.

The calculation of the signal prediction is based on a method proposed in [31]. The neutrino flux depends on the fission fractions of the uranium and plutonium isotopes in the reactor: ^{235}U , ^{238}U , ^{239}Pu and ^{241}Pu , respectively. The average contribution of these isotopes to the flux during data collection with reactor on is 53%, 8%, 32% and 7%. In principle, there is no energy threshold for the $\text{CE}\nu\text{NS}$ interaction itself and therefore there is a potential to measure neutrinos even below the threshold for the inverse beta decay reaction of about 1.8 MeV. Beyond the reactor conditions and its thermal power, the neutrino rate measured in the detector strongly depends on dissipation processes in the germanium crystals. The ionization energy observed in the detector is reduced with respect to the deposited recoil energy, a characteristic known as quenching. There was a debate, if this quenching factor is enhanced at low energies as compared to the Lindhard theory [32, 33]. From CONUS data, there is no indication of any deviation from the Lindhard model [27, 34].

A significant contribution to the systematic uncertainty is related to the precision of the energy scale calibration. At very low energies close to the energy region of interest, X-rays emitted in radioactive decays inside the detector crystals are used for calibration purposes. There are prominent lines around 10.4 keV corresponding to the binding energies of the K-shells and around 1.3 keV from L-shells of Ge isotopes, as seen in the left plot of Fig.2. Toward the end of the first data collection period in CONUS+, the detectors were irradiated with neutrons from a californium source outside the shield to increase the statistics in the corresponding lines and reduce the uncertainty of the energy scale to less than 5 eV. Small energy non-linearity effects close to the detection threshold induced by the data acquisition system [34] were measured with a pulse generator and corrected accordingly.

The energy threshold of the detectors is estimated for each of them individually [28]. The lowest value for the C3 detector is only 160 eV. For the other two detectors used in the analysis, the thresholds after energy non-linearity correction were set slightly above, at 170 eV and 180 eV. One of the four detectors (C4) showed significant instabilities in the rate and was therefore removed from the data set. The thresholds were defined in a way to assure that contributions from electronic noise and microphonics are negligible in the region of interest. The trigger efficiency was determined for each detector using a pulse generator and was found to be close to 100% above the thresholds.

Another crucial requirement for detecting CE ν NS at a nuclear reactor is the stability of environmental parameters, electronic noise and background rates. For example, temperature fluctuations can induce cryocooler power variations, which might create microphonic events. Microphonic noise and rate correlations with room temperature were further reduced compared to previous analyses [18, 27] by an improved cooling system [28]. The stability of the detector parameters such as energy resolution or trigger efficiency was regularly checked with the pulse generator. Variations of the noise peak were carefully monitored and data were only selected for the analysis in case they were below a defined level.

The data set used in the analysis reported here includes reactor on periods between November 2023 and July 2024 (327 kg d) and a off period during reactor outage in May 2024 (60 kg d). The data sets of the three detectors are fitted simultaneously in an energy window between 160 eV and 800 eV. The signal is extracted based on a profile likelihood ratio test. Systematic uncertainties are considered with Gaussian pull terms. The data acquisition system in principle allows for background rejection by studying the shape of digitized pulses [35]. This option was not yet applied in the current analysis, but it is planned to be used in future analyses.

From the combined fit, a neutrino signal of (395 ± 106) events in the reactor on data set was obtained. The significance of this event excess corresponds to 3.7σ . The neutrino signal at low energies of the spectrum is illustrated in Fig.3. Fits using just single detectors independently give consistent results. The result was cross-checked in two implementations of the likelihood fit and agreed within less than 2%. Additional systematic uncertainties related to background model, non-linearity correction and fit systematics were studied independently and are included in the fit result.

Impact and outlook

The CONUS+ signal of (395 ± 106) measured neutrinos is fully consistent with the expectation of (347 ± 59) events. This implies agreement of the CONUS+ data with the CE ν NS cross-section of the SM and the estimated antineutrino flux based on the thermal power of the reactor. Moreover, the detected rate is in very good agreement with the predicted Ge quenching using the Lindhard theory with a quenching parameter as measured in [34]. The deviations from Lindhard theory claimed in [33] and the excess reported in [17], which is based on it, are both ruled out by this result. The claim was already disfavored before by the independent measurement of the quenching factor [34], previous CONUS results [27] and theoretical considerations [36].

In Table 1, the ratio of measured and predicted neutrino interactions is shown for the CONUS+ result. This ratio is compared to the ratios measured in the COHERENT measurements at higher neutrino energies using multiple target nuclei and the results from coherent scattering of solar neutrinos. The use of different target nuclei allows to study the quadratic enhancement of the cross-section by the number of neutrons in the target. In the COHERENT data for Ge, the measured rate was found slightly below the predicted value, although not highly significant. Such a deficit was not confirmed in the CONUS+ data. The combination of the CE ν NS result of CONUS+ with results

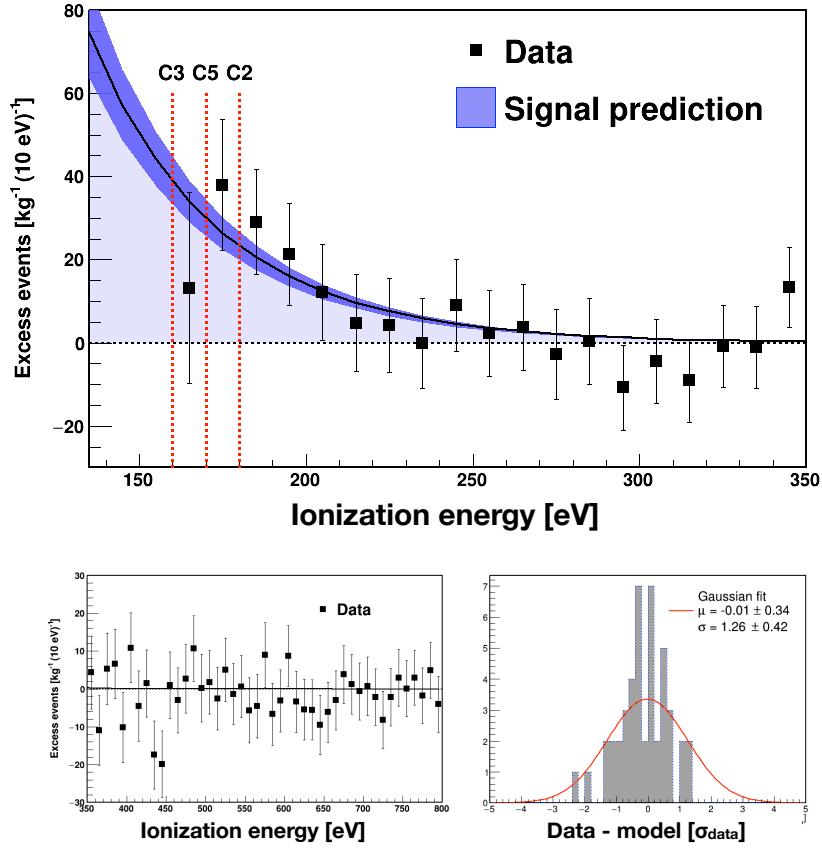


Fig. 3: The plot on top shows the difference between data in the full reactor on time and the background model scaled to the total detector mass. At low energies the rise from the neutrino signal can be seen. The line shows the predicted signal shape including uncertainties for comparison. The vertical lines indicate the energy thresholds of the three detectors used in the analysis. In the first bin only C3 contributes, in the second C3+C5 and above 180 eV all three detectors. On the bottom left, there is an extension of the top plot showing the good agreement between data and background model above the signal region from 350 – 800 eV. The histogram on the bottom right shows the corresponding spread of the data points around the model.

of the germanium target data of the COHERENT experiment can in principle be used to extract information about nuclear form factors in neutrino light.

After the first detection of $CE\nu NS$ at a nuclear reactor, as reported in this article, the next step will be a more precise measurement of the $CE\nu NS$ cross-section. Higher precision can be achieved by increasing the target mass, lowering the energy threshold of the detectors and longer operation times, in particular in the reactor off phases. Therefore, 3 of the 4 CONUS+ detectors were replaced in November 2024 by

Table 1: Comparison with other CE ν NS measurements.

Source	Target	ν energy [MeV]	flux [$\text{cm}^{-2}\text{s}^{-1}$]	data	data/SM prediction
Accelerator [37]	Cs	$\sim 10 - 50$	$5 \cdot 10^7$	306 ± 20	0.90 ± 0.15
Accelerator [3]	Ar	$\sim 10 - 50$	$2 \cdot 10^7$	140 ± 40	1.22 ± 0.37
Accelerator [38]	Ge	$\sim 10 - 50$	$5 \cdot 10^7$	21 ± 7	0.59 ± 0.21
Sun [24]	Xe	< 15	$5 \cdot 10^6$	11 ± 4	0.90 ± 0.45
Sun [25]	Xe	< 15	$5 \cdot 10^6$	4 ± 1	1.25 ± 0.52
Reactor	Ge	< 10	$1.5 \cdot 10^{13}$	395 ± 106	1.14 ± 0.36

a newer generation. These new detectors have a larger mass of 2.4 kg each. First characterizations in the MPIK laboratory indicated even lower energy thresholds. The detector with the lowest energy threshold in the first CONUS+ run (C3) was kept as a reference for a better comparison between the phases of the experiment. With this detector configuration it is planned to measure for another few years.

A high-statistics CE ν NS measurement might open a new phase in fundamental physics and will allow to study physics within and beyond the SM. The measured CE ν NS rate can for example be affected by new mediator particles similar to the Z boson, electromagnetic properties of neutrinos, or non-standard interactions. Moreover, it is possible to study the Weinberg angle at low energies, the existence of sterile neutrinos or supernovae astrophysics. There are also connections to dark matter experiments. A precise CE ν NS measurement will allow to learn more about the neutrino sources as the Sun or nuclear reactors. The evolution of the reactor thermal power and fissile isotope concentrations in fuel elements could be monitored with rather small and mobile neutrino detectors. In summary, there is a wide range of topics ranging from BSM theories, nuclear physics and astrophysics that can be addressed with CE ν NS measurements at nuclear reactors. The CONUS and CONUS+ experiments are pioneering in this field.

Acknowledgments

We thank all divisions and workshops involved at the Max-Planck-Institut für Kernphysik in Heidelberg to set up the CONUS+ experiment, in particular T. Apfel, M. Reissfelder, T. Frydlewicz and J. Schreiner. We also thank Mirion Technologies (Canberra) in Lingolsheim for the detector upgrades and their highly professional support. Our deepest gratitude goes to the Leibstadt AG for hosting and supporting the CONUS+ experiment with special thanks to P. Graf, P. Kaiser, L. Baumann, R. Meili and A. Ritter.

References

- [1] Freedman, D.Z.: Coherent Neutrino Nucleus Scattering as a Probe of the Weak Neutral Current. Phys. Rev. D **9**, 1389–1392 (1974) <https://doi.org/10.1103/PhysRevD.9.1389>

- [2] Akimov, D., *et al.*: Observation of Coherent Elastic Neutrino-Nucleus Scattering. *Science* **357**(6356), 1123–1126 (2017) <https://doi.org/10.1126/science.aao0990> [arXiv:1708.01294](https://arxiv.org/abs/1708.01294) [nucl-ex]
- [3] Akimov, D., *et al.*: First Measurement of Coherent Elastic Neutrino-Nucleus Scattering on Argon. *Phys. Rev. Lett.* **126**(1), 012002 (2021) <https://doi.org/10.1103/PhysRevLett.126.012002> [arXiv:2003.10630](https://arxiv.org/abs/2003.10630) [nucl-ex]
- [4] Adamski, S., *et al.*: First detection of coherent elastic neutrino-nucleus scattering on germanium (2024) [arXiv:2406.13806](https://arxiv.org/abs/2406.13806) [hep-ex]
- [5] Cowan, C.L., Reines, F., Harrison, F.B., Kruse, H.W., McGuire, A.D.: Detection of the free neutrino: A Confirmation. *Science* **124**, 103–104 (1956) <https://doi.org/10.1126/science.124.3212.103>
- [6] Abe, S., *et al.*: Precision Measurement of Neutrino Oscillation Parameters with KamLAND. *Phys. Rev. Lett.* **100**, 221803 (2008) <https://doi.org/10.1103/PhysRevLett.100.221803> [arXiv:0801.4589](https://arxiv.org/abs/0801.4589) [hep-ex]
- [7] An, F.P., *et al.*: Precision Measurement of Reactor Antineutrino Oscillation at Kilometer-Scale Baselines by Daya Bay. *Phys. Rev. Lett.* **130**(16), 161802 (2023) <https://doi.org/10.1103/PhysRevLett.130.161802> [arXiv:2211.14988](https://arxiv.org/abs/2211.14988) [hep-ex]
- [8] Kerret, H., *et al.*: Double Chooz θ_{13} measurement via total neutron capture detection. *Nature Phys.* **16**(5), 558–564 (2020) <https://doi.org/10.1038/s41567-020-0831-y> [arXiv:1901.09445](https://arxiv.org/abs/1901.09445) [hep-ex]
- [9] Bak, G., *et al.*: Measurement of Reactor Antineutrino Oscillation Amplitude and Frequency at RENO. *Phys. Rev. Lett.* **121**(20), 201801 (2018) <https://doi.org/10.1103/PhysRevLett.121.201801> [arXiv:1806.00248](https://arxiv.org/abs/1806.00248) [hep-ex]
- [10] Almazán, H., *et al.*: STEREO neutrino spectrum of ^{235}U fission rejects sterile neutrino hypothesis. *Nature* **613**(7943), 257–261 (2023) <https://doi.org/10.1038/s41586-022-05568-2> [arXiv:2210.07664](https://arxiv.org/abs/2210.07664) [hep-ex]
- [11] Andriamirado, M., *et al.*: Improved short-baseline neutrino oscillation search and energy spectrum measurement with the PROSPECT experiment at HFIR. *Phys. Rev. D* **103**(3), 032001 (2021) <https://doi.org/10.1103/PhysRevD.103.032001> [arXiv:2006.11210](https://arxiv.org/abs/2006.11210) [hep-ex]
- [12] Alekseev, I., *et al.*: Search for sterile neutrinos at the DANSS experiment. *Phys. Lett. B* **787**, 56–63 (2018) <https://doi.org/10.1016/j.physletb.2018.10.038> [arXiv:1804.04046](https://arxiv.org/abs/1804.04046) [hep-ex]
- [13] Atif, Z., *et al.*: Search for sterile neutrino oscillations using RENO and NEOS data. *Phys. Rev. D* **105**(11), 111101 (2022) <https://doi.org/10.1103/PhysRevD.105.L111101> [arXiv:2011.00896](https://arxiv.org/abs/2011.00896) [hep-ex]

- [14] Aguilar-Arevalo, A., *et al.*: Search for coherent elastic neutrino-nucleus scattering at a nuclear reactor with CONNIE 2019 data. *JHEP* **05**, 017 (2022) [https://doi.org/10.1007/JHEP05\(2022\)017](https://doi.org/10.1007/JHEP05(2022)017) arXiv:2110.13033 [hep-ex]
- [15] Alekseev, I., *et al.*: First results of the ν GeN experiment on coherent elastic neutrino-nucleus scattering. *Phys. Rev. D* **106**(5), 051101 (2022) <https://doi.org/10.1103/PhysRevD.106.L051101> arXiv:2205.04305 [nucl-ex]
- [16] Angloher, G., *et al.*: Exploring CE ν NS with NUCLEUS at the Chooz nuclear power plant. *Eur. Phys. J. C* **79**(12), 1018 (2019) <https://doi.org/10.1140/epjc/s10052-019-7454-4> arXiv:1905.10258 [physics.ins-det]
- [17] Colaresi, J., Collar, J.I., Hossbach, T.W., Lewis, C.M., Yocum, K.M.: Measurement of Coherent Elastic Neutrino-Nucleus Scattering from Reactor Antineutrinos. *Phys. Rev. Lett.* **129**(21), 211802 (2022) <https://doi.org/10.1103/PhysRevLett.129.211802> arXiv:2202.09672 [hep-ex]
- [18] Bonet, H., *et al.*: Constraints on elastic neutrino nucleus scattering in the fully coherent regime from the CONUS experiment. *Phys. Rev. Lett.* **126**(4), 041804 (2021) <https://doi.org/10.1103/PhysRevLett.126.041804> arXiv:2011.00210 [hep-ex]
- [19] Augier, C., *et al.*: Ricochet Progress and Status. *J. Low Temp. Phys.* **212**, 127–137 (2023) <https://doi.org/10.1007/s10909-023-02971-5> arXiv:2111.06745 [physics.ins-det]
- [20] Kerman, S., Sharma, V., Deniz, M., Wong, H.T., Chen, J.-W., Li, H.B., Lin, S.T., Liu, C.-P., Yue, Q.: Coherency in Neutrino-Nucleus Elastic Scattering. *Phys. Rev. D* **93**(11), 113006 (2016) <https://doi.org/10.1103/PhysRevD.93.113006> arXiv:1603.08786 [hep-ph]
- [21] Choi, J.J., *et al.*: Exploring coherent elastic neutrino-nucleus scattering using reactor electron antineutrinos in the NEON experiment. *Eur. Phys. J. C* **83**(3), 226 (2023) <https://doi.org/10.1140/epjc/s10052-023-11352-x> arXiv:2204.06318 [hep-ex]
- [22] Yang, L.T., Liang, Y.F., Yue, Q.: RECODE program for reactor neutrino CE ν NS detection with PPC Germanium detector. *PoS TAUP2023*, 296 (2024) <https://doi.org/10.22323/1.441.0296>
- [23] Akimov, D.Y., *et al.*: First constraints on the coherent elastic scattering of reactor antineutrinos off xenon nuclei (2024) arXiv:2411.18641 [hep-ex]
- [24] Aprile, E., *et al.*: First Indication of Solar B8 Neutrinos via Coherent Elastic Neutrino-Nucleus Scattering with XENONnT. *Phys. Rev. Lett.* **133**(19), 191002 (2024) <https://doi.org/10.1103/PhysRevLett.133.191002> arXiv:2408.02877 [nucl-ex]

- [25] Bo, Z., *et al.*: First Indication of Solar B8 Neutrinos through Coherent Elastic Neutrino-Nucleus Scattering in PandaX-4T. *Phys. Rev. Lett.* **133**(19), 191001 (2024) <https://doi.org/10.1103/PhysRevLett.133.191001> arXiv:2407.10892 [hep-ex]
- [26] Bonet, H., *et al.*: Large-size sub-keV sensitive germanium detectors for the CONUS experiment. *Eur. Phys. J. C* **81**(3), 267 (2021) <https://doi.org/10.1140/epjc/s10052-021-09038-3> arXiv:2010.11241 [physics.ins-det]
- [27] Ackermann, N., *et al.*: Final CONUS Results on Coherent Elastic Neutrino-Nucleus Scattering at the Brokdorf Reactor. *Phys. Rev. Lett.* **133**(25), 251802 (2024) <https://doi.org/10.1103/PhysRevLett.133.251802> arXiv:2401.07684 [hep-ex]
- [28] Ackermann, N., *et al.*: CONUS+ Experiment. *Eur. Phys. J. C* **84**(12), 1265 (2024) <https://doi.org/10.1140/epjc/s10052-024-13551-6> arXiv:2407.11912 [hep-ex]
- [29] Bonet, H., *et al.*: Full background decomposition of the CONUS experiment. *Eur. Phys. J. C* **83**(3), 195 (2023) <https://doi.org/10.1140/epjc/s10052-023-11240-4> arXiv:2112.09585 [physics.ins-det]
- [30] Sanchez Garcia, E., *et al.*: Background characterization of the CONUS+ experimental location (2024) arXiv:2412.13707 [physics.ins-det]
- [31] An, F.P., *et al.*: Antineutrino energy spectrum unfolding based on the Daya Bay measurement and its applications. *Chin. Phys. C* **45**(7), 073001 (2021) <https://doi.org/10.1088/1674-1137/abfc38> arXiv:2102.04614 [hep-ex]
- [32] Lindhard, J., Scharff, M., Schiøtt, H.E.: Range Concepts and Heavy Ion Ranges. *Matematisk-fysiske meddelelser*. Munksgaard (1963). <https://books.google.de/books?id=M2ymQEACAAJ>
- [33] Collar, J.I., Kavner, A.R.L., Lewis, C.M.: Germanium response to sub-keV nuclear recoils: a multipronged experimental characterization. *Phys. Rev. D* **103**(12), 122003 (2021) <https://doi.org/10.1103/PhysRevD.103.122003> arXiv:2102.10089 [nucl-ex]
- [34] Bonhomme, A., *et al.*: Direct measurement of the ionization quenching factor of nuclear recoils in germanium in the keV energy range. *Eur. Phys. J. C* **82**(9), 815 (2022) <https://doi.org/10.1140/epjc/s10052-022-10768-1> arXiv:2202.03754 [physics.ins-det]
- [35] Bonet, H., *et al.*: Pulse shape discrimination for the CONUS experiment in the keV and sub-keV regime. *Eur. Phys. J. C* **84**(2), 139 (2024) <https://doi.org/10.1140/epjc/s10052-024-12470-w> arXiv:2308.12105 [physics.ins-det]
- [36] Atzori Corona, M., Cadeddu, M., Cargioli, N., Dordei, F., Giunti, C.: On the

- impact of the Migdal effect in reactor CE ν NS experiments. Phys. Lett. B **852**, 138627 (2024) <https://doi.org/10.1016/j.physletb.2024.138627> arXiv:2307.12911 [hep-ph]
- [37] Akimov, D., *et al.*: Measurement of the Coherent Elastic Neutrino-Nucleus Scattering Cross Section on CsI by COHERENT. Phys. Rev. Lett. **129**(8), 081801 (2022) <https://doi.org/10.1103/PhysRevLett.129.081801> arXiv:2110.07730 [hep-ex]
- [38] Adamski, S., *et al.*: First detection of coherent elastic neutrino-nucleus scattering on germanium (2024) arXiv:2406.13806 [hep-ex]
- [39] Boswell, M., *et al.*: MaGe-a Geant4-based Monte Carlo Application Framework for Low-background Germanium Experiments. IEEE Trans. Nucl. Sci. **58**, 1212–1220 (2011) <https://doi.org/10.1109/TNS.2011.2144619> arXiv:1011.3827 [nucl-ex]
- [40] Goldhagen, P., Clem, J.M., Wilson, J.W.: The energy spectrum of cosmic-ray induced neutrons measured on an airplane over a wide range of altitude and latitude. Radiation Protection Dosimetry **110**(1-4), 387–392 (2004) <https://doi.org/10.1093/rpd/nch216>
- [41] Gordon, M.S., Goldhagen, P., Rodbell, K.P., Zabel, T.H., Tang, H.H.K., Clem, J.M., Bailey, P.: Measurement of the flux and energy spectrum of cosmic-ray induced neutrons on the ground. IEEE Transactions on Nuclear Science **51**(6), 3427–3434 (2004) <https://doi.org/10.1109/TNS.2004.839134>
- [42] Bugaev, E.V., Misaki, A., Naumov, V.A., Sinigovskaya, T.S., Sinigovsky, S.I., Takahashi, N.: Atmospheric muon flux at sea level, underground, and underwater. Phys. Rev. D **58**, 054001 (1998) <https://doi.org/10.1103/PhysRevD.58.054001>
- [43] Reyna, D.: A simple parameterization of the cosmic-ray muon momentum spectra at the surface as a function of zenith angle (2006) arXiv:hep-ph/0604145 [hep-ph]

Supplemental material

Data taking

Data from the CONUS+ run 1 analysis presented in this publication correspond to the period from November 2023 to July 2024. Three of the four detectors, named C2, C3, and C5, are considered for analysis with a total active mass of 2.83 ± 0.02 kg [26]. After selection cuts to remove time periods with unstable noise conditions, deficient radon flushing, and a few days with a strong contribution of microphonic events, the exposure considering the active mass is 327 kg days with reactor on and 60 kg days with the reactor off.

The evolution of the main environmental parameters during reactor on and off is shown in figure 4-left, figure 4-center and figure 4-right, for the C5, C2, and C3 detectors, respectively. The excluded data periods are depicted (red-shadow area). The shape of the noise peak reconstructed in the lowest channels of the data acquisition system (DAQ) was found to follow a Gaussian distribution [28] and its width (FWHM) was monitored over time with variations below $2 eV_{ee}$ (electron equivalent energy). The data set was selected to ensure that the noise rate variations are below 20%. Variations in the cryocooler power are not solely caused by changes in room temperature. They were also induced by instabilities in the recirculation of the cooling liquid, an issue that was solved for run 2 in CONUS+.

Detector response and energy scale

The trigger efficiency was determined by injecting artificial signals produced by a pulse generator with the same rise time as the physical signals. A detailed scan allowed us to measure the detector response as a function of the energy. The description of the experimental trigger efficiency curves is depicted in [28] and was obtained using the fit function:

$$\varepsilon_{trig} = 0.5 \cdot \left(1 + \operatorname{erf} \left(\frac{E_{ee}/eV_{ee} - t_1}{t_2} \right) \right), \quad (1)$$

with t_1 being a value in [99, 109] and t_2 in [51, 54], respectively. In particular, the trigger efficiency remains over 90% down to 140 eV_{ee} for all detectors. The evolution of the trigger efficiency curve parameters during run 1 was studied with different measurements, remaining stable with differences of less than 2% throughout the run.

Proper energy calibration is fundamental for achieving a precise neutrino measurement. The energy was calibrated using the binding energies of the K shell (10.37 keV) and L shell (1.30 keV) from the decays of ^{71}Ge inside the HPGe diodes, considering a linear behavior in this energy range. The ^{71}Ge is created by the capture of neutrons up to a few MeV energy. The half-life of ^{71}Ge is 11.4 d, so a few weeks of data collection is enough to record most of the decays of ^{71}Ge after activation. The ^{71}Ge radioisotope is also continuously produced at shallow depth by neutrons released in muon interactions with Pb of the CONUS+ shield [28]. Thus, it is possible to monitor the stability of the energy scale during the whole measurement of this in situ activation, observing variations below 2%. A specific ^{252}Cf irradiation was performed at the

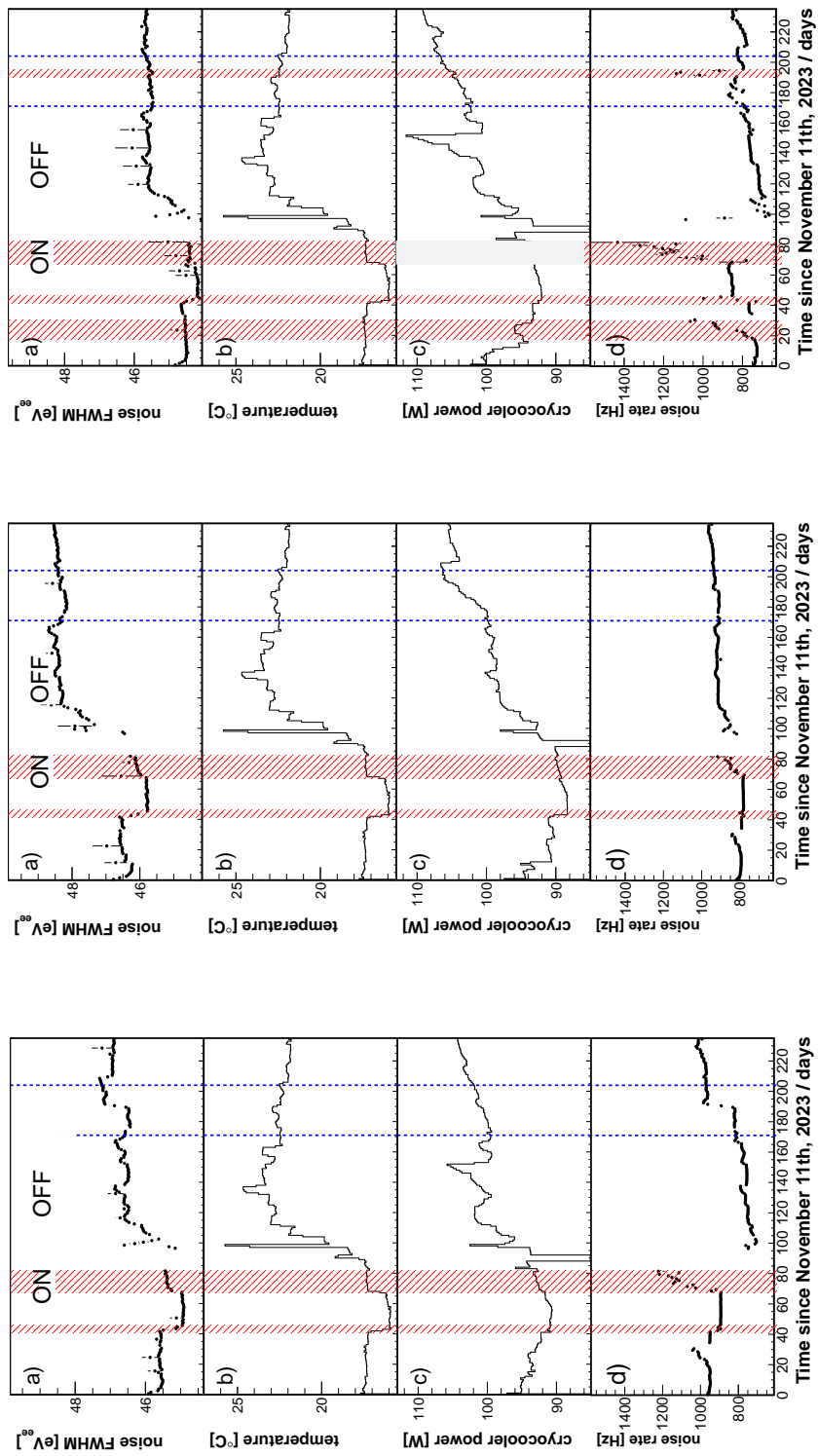


Fig. 4: Evolution of parameters for the C5 (left), C2(center), and C4 (right) detectors during run 1. From top to bottom: a) FWHM of noise peak, b) air temperature close to the detector preamplifier, c) cryocooler power consumption, and d) event trigger rate. Red areas were excluded from the analysis, and blue dashed lines indicate the period of reactor outage.

end of run 1, collecting in 45 d of the measurement more than 5000 (700) events from the K (L) shell in each detector. In this way, an energy calibration uncertainty below 5 eV_{ee} is achieved. The HPGe diode also produces 158 eV X-rays from the binding energy of the M shell of the ⁷¹Ge decays. Using the ratio of the K and L shells, a total of 100 events per detector was expected after irradiation with ²⁵²Cf. Although an indication of such events is seen, no conclusive signal was yet observed due to the proximity to the noise edge and the lack of statistics. Future irradiation after upgrades is planned to measure the M shell line in the CONUS+ detectors.

The linearity of the DAQ chain in the sub-keV_{ee} region was investigated by injecting artificial pulser signals. The results are shown in figure 5. Deviations from a pure linear behavior are observed below 250 eV_{ee}, where a few eV_{ee} variations have a strong impact on the CEνNS signal. They were attributed to two nearly independent DAQ-related effects. First, as the amplitude of the signals decreases, artificial delays of the trigger time stamp were observed up to a few μs. Due to the relatively short shaping time of 4 μs, these delays affect the reconstructed energy value obtained by trapezoidal shaping. The corresponding negative non-linearity effect reaches its maximum of approximately 15 eV_{ee} at 120 eV_{ee}. Second, the drop in trigger efficiency below 120 eV_{ee} is responsible for an artificial positive deviation from linearity, overwhelming the above-mentioned effect. This effect was also observed in [34]. The energy non-linearity was corrected in the CEνNS analysis and was taken into account during the event energy reconstruction.

The energy resolution of the detectors at low energies was evaluated using artificial signals generated by a pulse generator with the same pulse rise time as the physical signals. The pulses are injected through a specific circuit implemented in the HPGe preamplifier. For the C2 detector, a pulser resolution of (48 ± 1) eV_{ee} (FWHM) was found, while the C5 and C3 detectors have a pulser resolution of (47 ± 1) eV_{ee} (FWHM). An additional contribution to the total energy resolution comes from the statistical fluctuation of the number of electron-hole pairs produced in the Germanium crystals in the case of an event. This contribution is

$$\Delta E_S = 2.35\sqrt{F\epsilon E} \quad (2)$$

with $\epsilon = 2.96$ eV, the average energy needed to create a single electron-hole pair in Germanium, and the fano factor F. For this analysis a value of $F = 0.1096$ was used.

Selection cuts

The spectrum in the HPGe detectors is dominated by background events (mainly produced by muon-induced neutrons). Selection cuts are applied to reduce the background while keeping the CEνNS signal. Four different selection cuts are applied to the data: First, the muon-veto system allows for efficient suppression of the impact of cosmic radiation, using a 450 μs anti-coincidence window between the veto and HPGe signals. The average rate detected in the muon veto during reactor ON is (274 ± 1) Hz and decreases to (214 ± 1) Hz in reactor off periods. For this reason, the dead time induced by the muon veto system was independently estimated for both periods with

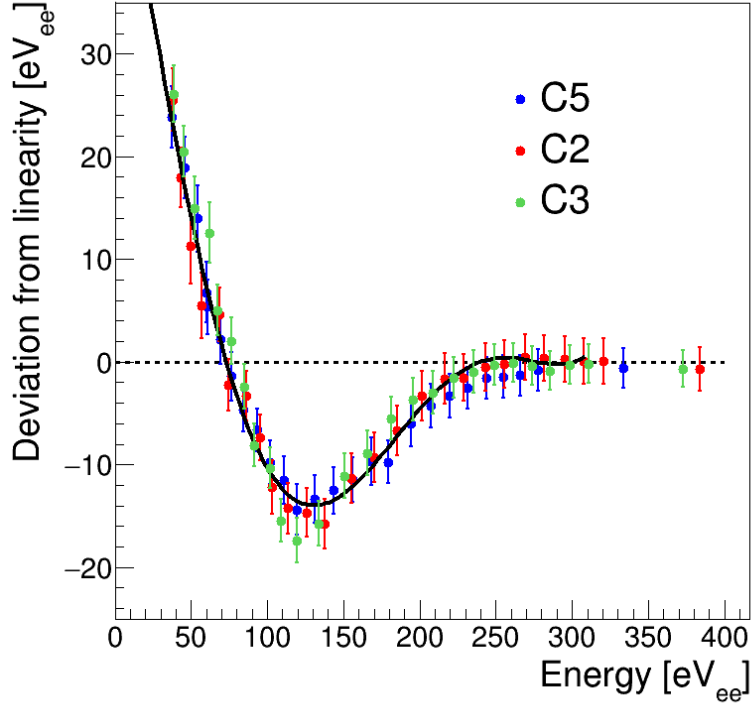


Fig. 5: Deviations from a purely linear energy scale measured with a pulse generator for the three CONUS+ detectors. The points are described by the black line.

average values of 12.3% (reactor on) and 9.6% (reactor off). This cut successfully suppressed the background with a rejection efficiency of more than 99% in most of the energy range.

Second, inhibit signals are generated when the increasing baseline has reached saturation of the dynamic range of the transistor reset preamplifier (TRP) for each HPGe detector [28]. An anti-coincidence window of 1 to 2.5 ms (depending on the detector) is applied to veto unwanted spurious HPGe detector signals generated shortly after the resets. This cut suppressed 30% events after the muon veto anti-coincidence at low energy, becoming negligible above 5 keV_{ee}. The dead time induced by this cut is calculated combined with the previously mentioned muon-veto dead time to avoid the overlapping of both veto windows. An additional dead time of 0.5-2.1% (depending on the detector) is estimated.

Third, the time difference distribution (TDD) of events is studied in each channel as proposed in [26]. In this way, noise events from failures in the pile-up cut of the DAQ and from microphonics are efficiently removed with nearly no loss in live time.

Finally, an anti-coincidence cut is applied between different HPGe detectors with a 5 ms time window. The probability of a neutrino interacting with different detectors

Table 2: The efficiency of all the selection cuts applied during the data processing. The efficiency of each cut is calculated with respect to the previous selection applied. Two energy ranges are considered between [0.4-1] keV_{ee} and [2-8] keV_{ee} to avoid the inclusion of background lines and the antineutrino signal. A combined efficiency of over 99% is achieved for all detectors.

[0.4-1.0] keV _{ee}						
Detector	C5		C2		C3	
Reactor period	On	Off	On	Off	On	Off
muon veto anti.	99.3%	99.3%	99.8%	99.8%	99.8%	99.8%
TRP anti.	35.9%	39.6%	43.4%	44.0%	43.9%	46.5%
TDD	0.1%	0.1%	0.2%	0.5%	0.2%	0.1%
neutron anti.	6.8%	6.6%	4.3%	4.8%	7.2%	6.8%
combined	99.6%	99.6%	99.9%	99.9%	99.9%	99.9%
[2-8] keV _{ee}						
Detector	C5		C2		C3	
Reactor period	On	Off	On	Off	On	Off
muon veto anti.	98.9%	98.9%	98.6%	98.6%	98.7%	98.9%
TRP anti.	19.7%	25.0%	3.9%	5.5%	6.1%	6.7%
TDD	0.1%	0.1%	0.1%	0.1%	0.1%	0.1%
neutron anti.	6.5%	7.0%	4.3%	4.3%	6.7%	6.5%
combined	99.2%	99.2%	99.1%	99.1%	98.9%	99.1%

is negligible, while for other backgrounds, such as muon-induced neutrons created in the shield, simultaneous hits in several detectors at once can be expected. This cut suppresses about 5% of the background after the muon veto anti-coincidence in the [0.4-1] keV_{ee} energy range without inducing a significant amount of dead time. The measured suppression efficiency is in good agreement with the background simulations.

The rejection efficiencies of these selection cuts during reactor on and off are summarized in table 2 for the C5, C2, and C3 detectors in different energy regions. A total rejection efficiency over 99% is achieved in the [0.4-1] keV_{ee} energy range for all detectors. The total dead time induced by the selection cuts is dominated by the muon veto anti-coincidence with values between 12.8% and 14.4% in the reactor on periods. In addition, the average dead time induced by the DAQ is calculated to be below 2%.

Background model

The background model used in the analysis of the CONUS+ data is based on Monte Carlo simulations using the Geant4-based framework MaGe [39]. With this framework, three categories of possible backgrounds were investigated following the approach taken in [29]:

1. Cosmogenic components (Muons and neutrons)
2. Natural radioactivity (external and internal to shield)
3. Artificial components (Reactor-correlated components, surface contaminations)

In general, a full decomposition of the background in both, reactor on and off data was achieved for all three detectors used in the analysis. In the following section, the major sources of background will be described in more detail.

Cosmogenic neutrons

As described in [30], the impact of cosmogenic neutrons with energies up to 100 MeV was investigated by first propagating the expected neutron spectrum at the KKL location (based on [40],[41]) with a flux of $(1.4 \pm 0.2) \cdot 10^{-2}$ neutrons $s^{-1}cm^{-2}$ through a model of the reactor building. Then the resulting flux is tracked inside the CONUS+ room. This flux was used as the basis for a next simulation, in which neutrons were started isotropically from a half-sphere around the CONUS+ shield and their contribution to the CONUS+ background was measured. The simulations show a contribution of (21.6 ± 3.1) counts $d^{-1}kg^{-1}$ in each detector in the energy range between 0.4 keV_{ee} and 1 keV_{ee} , which corresponds to approximately half of the background counts in this region, respectively.

Cosmogenic muons

For the muon simulations [29] the expected flux and muon spectrum at an overburden of 7.4 m w.e. were calculated from those at Earth's surface ([42],[43]) and propagated through the shield. The resulting spectrum was validated by comparing it to the CONUS+ data without the applied muon veto cut and good agreement was found. The muon veto cut was then applied by multiplying the simulation output by a factor of 0.01 for all energies greater than 2 keV_{ee} , corresponding to a muon veto efficiency of 99% for these energy regions.

For energies below 2 keV_{ee} a different approach was taken. Here, simulations show an inefficiency in the tagging ability of the muon veto system due to the setup of the shield. As shown in figure 1, the outer muon veto is located under a layer of lead in the CONUS+ shield. As such, it is possible that muons pass through this outermost lead layer without hitting one of the muon veto layers. These muons can induce electromagnetic showers in the outer lead layer, which propagate through the shield and are registered in the Germanium detectors. However, because no muon passes through any muon veto layer in such an event, the energy deposition in the plastic scintillator plates will be much lower, resulting in a greatly reduced tagging efficiency of these events. Simulations show that at very low energies (below 0.4 keV_{ee}) up to 80% of all muon-induced background come from such events. Based on this simulation output, this inefficiency was modeled with a polynomial and accounted for in the final muon veto efficiency below 2 keV_{ee} . The resulting efficiency drops towards lower energies with its minimum being 97% for energies below 0.4 keV_{ee} .

Using this approach, the overall background contribution of cosmic ray muons was found to be (17.4 ± 0.3) counts $d^{-1}kg^{-1}$ in each detector in the energy range between

0.4 keV_{ee} and 1 keV_{ee}, which corresponds to approximately a third of the background counts in this region, respectively.

Other background components

The remaining background in each detector is made up of many different components similar to the situation in Brokdorf (KBR) [29]. There are no hints that the detector upgrades or the movement of the setup were introducing any contamination. The background model includes cosmogenically induced isotopes in the Copper parts (⁵⁷Co, ⁶⁰Co, ⁵⁴Mn) of the cryostat and the Germanium crystals (⁵⁷Co, ⁶⁸Ge, ⁶⁸Ga, ⁶⁵Zn, ³H), Radon inside the detector chamber, ²¹⁰Pb inside the cryostat and shield, metastable germanium states (^{71m}Ge, ^{73m}Ge, ^{75m}Ge) and inert gases coming from the reactor (⁸⁵Kr, ¹³⁵Xe, ³H). The results of the simulation of these components were scaled to be in accordance with either the rates of gamma lines produced by the decay of these isotopes in the spectrum (e.g. for radon) or with screening measurements done prior to the installation. The listed contributions are typically very subdominant in the region of interest, with the decay of radon inside the detector chamber being the only exception. This contribution results in a background rate of (1.9 ± 0.1) counts d⁻¹kg⁻¹ between 0.4 keV_{ee} and 1 keV_{ee} for the C5 detector (C2: (2.8 ± 0.1) counts d⁻¹kg⁻¹; C3: (2.6 ± 0.1) counts d⁻¹kg⁻¹). The difference in radon contributions is likely due to the distribution of the radon decay products inside the detector chamber. As such, the C5 detector has the lowest radon component due to its proximity to the entry point of the radon free air. The listed values correspond to approximately 5% of the background in this energy region. Furthermore, radon decay has a high impact on energies above 100 keV_{ee}, where it can contribute up to 60% of the measured background. Slow pulses, arising from decays on the surface of the diode are included in the model [29].

Leakage test component

As previously described in [27], during the final run of the CONUS experiment in Brokdorf an additional background component had to be introduced in the background model. This component was present after ventilation of the cryostats with argon gas to avoid mechanical deformation during a regular leakage test at KBR in July 2019 [29]. Of the four detectors that were used in the CONUS experiment and were therefore affected by this additional background, two (C2 and C3) are used for the analysis presented in this work. Indeed, the simulations and the background model show that an additional component with the same shape is still present in the background of these two detectors but is absent in C5 which was not at KBR at the time. This additional background is constant during reactor on and off periods. Therefore, the leakage test component was again included in the background model of C2 and C3 by modeling it using a function with two parameters, as in [27]. The resulting impact is below 10% in the energy region between 0.4 keV_{ee} and 1 keV_{ee}.

Model differences in reactor off data

In addition to the background sources listed above, the background model of CONUS+ also accounts for experimental differences during data collection with the reactor off. The first of these differences is induced by the fact that during a reactor outage the head of the drywell, the containment structure immediately surrounding the core of the reactor, is placed directly above the CONUS+ room. This drywell head is made of 3.8 cm of steel and therefore increases the overburden of the experiment by approximately 0.3 m w.e. which results in a reduction of 19% in the flux of cosmogenic neutrons and a reduction of 3% in the cosmic ray muon flux. As a result, these two background contributions are reduced accordingly.

A second difference in the background model of the reactor off period comes from a more effective radon removal in the detector chamber. Over the course of run 1 shield tightness and flushing with radon free air were improved. As a result, the radon contribution in reactor off time is reduced by approximately a factor of 4 to 6 compared to reactor on. The radon contribution in the reactor off data was again scaled to match the count rate in the gamma lines induced by the radon decay.

In addition, reactor-correlated background components, such as reactor neutrons and high energy gammas, e.g. from ^{16}N , were investigated. Their impact was found to be negligible in all energy regions, including the region of interest. The resulting background model for all three detectors can be seen in figures 2 and figure 6.

In figure 7, the reactor on and off data sets are compared with the background models. If the calculated difference between on and off phases is added to the reactor off data, good agreement with the measured on data is found above the signal region. For all three detectors, good agreement was found between models and data for both reactor on (above 0.4 keV_{ee}) and reactor off phases (full spectrum). Since the data in the reactor off phase is statistically limited, the background model still has an important role in the analysis.

Table 3 gives an overview of the main background sources and their contribution in the energy range between 0.4 keV_{ee} and 1 keV_{ee} . A dedicated publication focusing on the full background decomposition is planned for the near future.

Quenching

The ratio of the ionization energy released by nuclear recoil in a $\text{CE}\nu\text{NS}$ event and the ionization energy of electrons of the same energy is given by the quenching factor. In the CONUS+ analysis, the energy dependent signal quenching is described by the Lindhard model [32] with a quenching parameter $k = (0.162 \pm 0.004)$ as determined in [34]. Alternative quenching descriptions are also tested as described in the supplemental material of [27] including a linear and cubic functional form to describe the increased quenching factor compared to Lindhard theory found in [33].

The signal predictions for the description of these different quenching models are shown in figure 8 together with the difference between the data in the reactor on phase and the background model. A signal rate of (2600 ± 300) events is expected for the linear function, while for the cubic function (550 ± 50) events are predicted. Both numbers are significantly higher than the neutrino rate extracted from the CONUS+

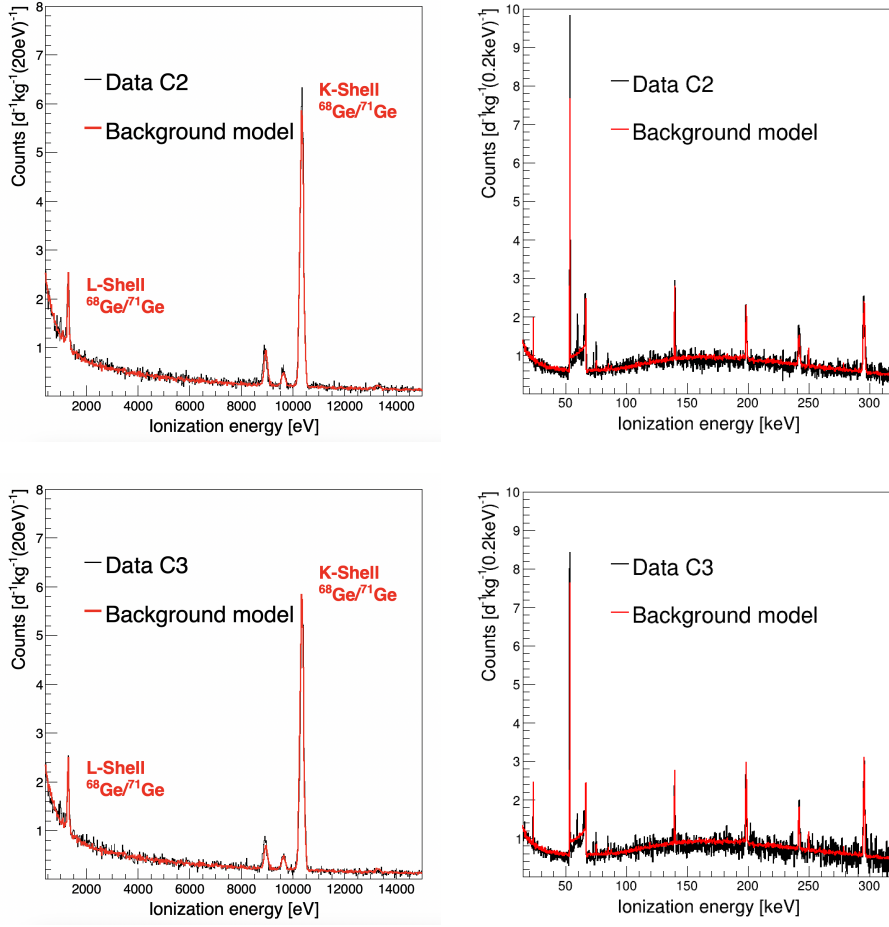


Fig. 6: Data and background model for the C2 and C3 detectors, equivalent to figure 2. Good agreement is found between data and model.

data. The standard Lindhard model clearly provides the best description of the reactor correlated excess at low energy. In figure 8 we have also included an additional data point at 200 eV_{ee} . This one is obtained using the information shown in figure 4 of [17]. There, a $\text{CE}\nu\text{NS}$ signal was approximated with an exponential using two parameters, the amplitude at 200 eV_{ee} ($A_{0,2}$) and a decay constant. The favored value for $A_{0,2}$ is shown within a 2σ contour in a 2-dimensional plot of the two parameters. We scaled this $A_{0,2}$ value to our exposure and corrected for the difference in neutrino flux. The value obtained was added in figure 8. As expected, it matches the description of Lindhard with a linear increase added at low energies but is in clear conflict with the CONUS+ data. The lower error bar corresponds to the smallest value of $A_{0,2}$ in the 2σ contour. This value is also clearly ruled out by the CONUS+ data points.

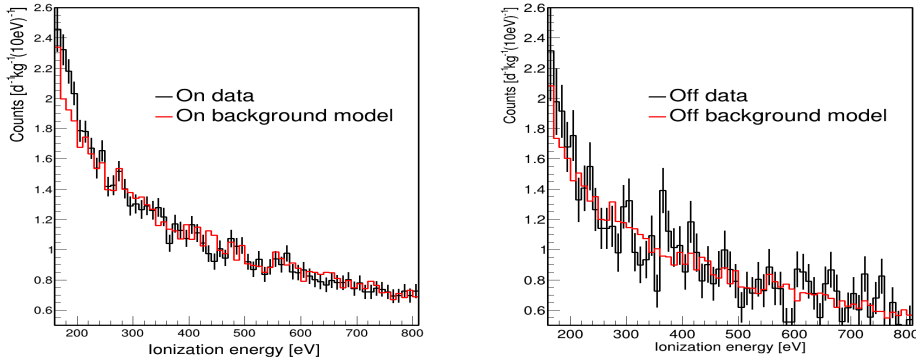


Fig. 7: Reactor on (left) and off (right) count rates normalized to 1 kg day in comparison to the corresponding background models are shown in the region of interest. The signal excess in the reactor on data is seen at low energies below 250 eV_{ee} . Statistical fluctuations are significantly higher in the off than in the on data due to the shorter period of data collection. Due to the slightly different detector thresholds only one detector (C3) contributes to the lowest bin, the second includes two detectors (C3 and C5) and bins above 180 eV_{ee} are based on the summed spectra of of all three detectors. The difference between the two reactor on curves on the left is shown in figure 3 which also includes the uncertainty of the background model.

Likelihood fit and systematics treatment

A likelihood function is used to determine the $\text{CE}\nu\text{NS}$ signal in the CONUS+ run 1 data.

$$\begin{aligned}
 -2 \log \mathcal{L} &= -2 \log \mathcal{L}_{\text{ON}} - 2 \log \mathcal{L}_{\text{OFF}} \\
 &+ \sum_{ij} (\theta_i - \bar{\theta}_i)^{\text{T}} \text{Cov}_{ij}^{-1} (\theta_j - \bar{\theta}_j) \\
 &+ \sum_i \frac{(\theta_i - \bar{\theta}_i)^2}{\sigma_{\theta_i}},
 \end{aligned} \tag{3}$$

\mathcal{L}_{ON} and \mathcal{L}_{OFF} are the likelihood functions for reactor on and off periods. Gaussian pull terms for the systematic uncertainties are also included. Here, the first term represents the pull terms for correlated parameters, namely the trigger efficiency parameters, and the second term represents pull terms for uncorrelated parameters, like the active mass of the detectors, the reactor neutrino flux and the uncertainty on the energy scale calibration of the spectra. Parameters that were experimentally determined are pulled to their measured values. A background scaling factor is also included.

Fits using just single detectors independently give consistent results as shown in Table 4. To cross-check the result, fits were performed by two independent likelihoods with different approaches concerning the uncertainty on the quenching model. Likelihood A applied a predicted $\text{CE}\nu\text{NS}$ spectrum with a fixed k parameter ($k = 0.162$)

Table 3: Overview of the major background components for all three detectors in reactor on and off measurements. All values are given in counts $\text{d}^{-1}\text{kg}^{-1}$.

[0.4-1.0] keV_{ee}						
Detector	C5		C2		C3	
Reactor period	On	Off	On	Off	On	Off
Cosmogenic neutrons	21.6 ± 3.1	17.7 ± 2.5	21.6 ± 3.1	17.7 ± 2.5	21.6 ± 3.1	17.7 ± 2.5
Cosmogenic muons	17.4 ± 0.3	16.9 ± 0.3	17.4 ± 0.3	16.9 ± 0.3	17.4 ± 0.3	16.9 ± 0.3
Radon	1.9 ± 0.1	0.3 ± 0.1	2.8 ± 0.1	0.7 ± 0.1	2.6 ± 0.1	0.7 ± 0.1
Other	2.0 ± 0.2	1.2 ± 0.2	6.4 ± 0.5	5.6 ± 0.5	5.6 ± 0.5	4.8 ± 0.5
Leakage test component	-	-	3.0 ± 0.5	3.0 ± 0.5	0.8 ± 0.2	0.8 ± 0.2
Total (Model)	42.9 ± 3.1	35.8 ± 2.5	52.3 ± 3.3	45.1 ± 2.7	49.3 ± 3.1	42.2 ± 2.7
Total (Data)	43.5 ± 1.1	33.4 ± 1.8	50.7 ± 1.2	45.3 ± 1.3	48.8 ± 1.2	42.5 ± 2.0

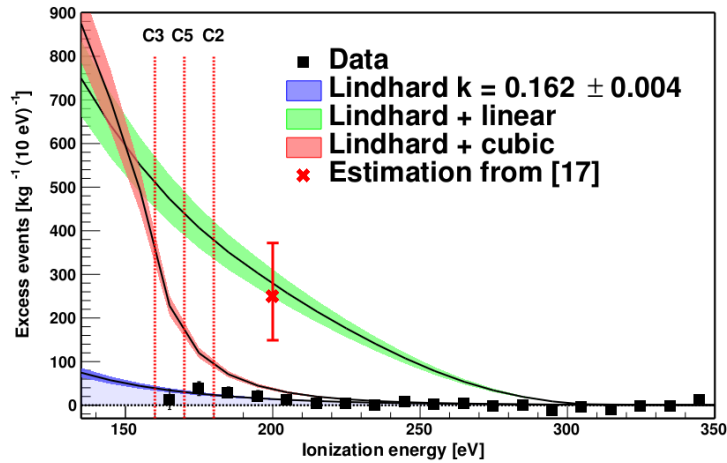


Fig. 8: Difference between the data in the reactor on phase and the background model normalized to the total detector mass. The blue band shows the predicted signal shape assuming the standard Lindhard model with a quenching factor of $k = (0.162 \pm 0.004)$ [34]. The green and red bands depict the signal predictions for the modified Lindhard model based on [33], using a linear and a cubic function at lower energies respectively. The vertical lines indicate the energy thresholds of the three detectors used in the analysis. The additional data point at 200eV_{ee} indicates the favored value found in [17] with an error bar reflecting the 2σ contour also presented in [17].

Table 4: Energy thresholds (E_{th}), reactor on live time and results are listed for the individual detectors and the combined fit. In the combined fit result, additional systematic uncertainties mainly from the non-linearity correction and background model are included. The calculated number of neutrino events in the region of interest and the ratio of prediction to data are given for 327 kg days of reactor on time.

Detector	E_{th} [eV_{ee}]	mass [kg]	live time	Signal events data	Signal predicted	Ratio
C2	180	0.95 ± 0.01	117 days	69 ± 47	96 ± 16	0.72 ± 0.50
C3	160	0.94 ± 0.01	110 days	186 ± 66	135 ± 23	1.38 ± 0.54
C5	170	0.94 ± 0.01	119 days	117 ± 75	116 ± 20	1.01 ± 0.67
combined		2.83 ± 0.02		395 ± 106	347 ± 59	1.14 ± 0.36

Table 5: Overview of uncertainties on the signal prediction and on the CE ν NS result.

Prediction uncertainties	
Uncertainty	Contribution
Energy threshold	14.1%
Quenching Ge	7.3%
Reactor neutrino flux	4.6%
Cross-section	3.2%
Active mass Ge	1.1%
Trigger efficiency	0.7%
All combined	17%
CE ν NS result uncertainties	
Uncertainty	Contribution
Likelihood fit	± 86
Fit method	± 7
Background model	± 40
Non-linearity implementation	± 47
All combined	± 106

while introducing a fourth order polynomial to vary the shape of the signal spectrum applying Gaussian pull terms on each parameter. In likelihood B, the k value of the Lindhard model is a fit parameter with a pull term. Moreover, there are some differences in the treatment of the non-linearity corrections and the minimization algorithms between the two likelihood fits. In the end, the results of both likelihood implementations agree within 2%.

The overview of the systematic uncertainties in signal prediction is summarized in table 5. To be conservative, we assume that all of them are fully correlated between single detectors. Currently, it is dominated by the $5 eV_{ee}$ uncertainty in the energy calibration. Future extended calibrations will allow us to improve this value to $3 eV_{ee}$, reducing the contribution of this systematic term. To achieve a total signal prediction uncertainty below 8% new improved quenching factor measurements would be needed.

The likelihood fit itself gives a result of (395 ± 86) CE ν NS counts in the combined fit of the three detectors. Additional systematic uncertainties not implemented as pull

terms are estimated in a second step and added in quadrature, giving the final uncertainty of ± 106 signal counts. The different contributions are listed in table 5. The biggest contribution comes from the likelihood fit, combining both statistic and systematic uncertainties considering the pull terms in the likelihood function. The second biggest impact is the uncertainty due to the implementation of the non-linearity correction, explained above. This is caused by the choice of a specific function to describe and fit the deviations from a purely linear energy scale in figure 5. This uncertainty was obtained through a systematic study of other possible fit functions and checking the impact on the likelihood result. An additional uncertainty from the background model description originates mainly from uncertainties on the muon and neutron flux in the CONUS+ room as well as the leakage component. The uncertainty was obtained by varying the background model within the model constraints and subsequently performing the likelihood fits. Lastly, the fit method itself, i.e. the difference between Likelihood A and B, as mentioned above, has a small additional impact on the overall uncertainty.

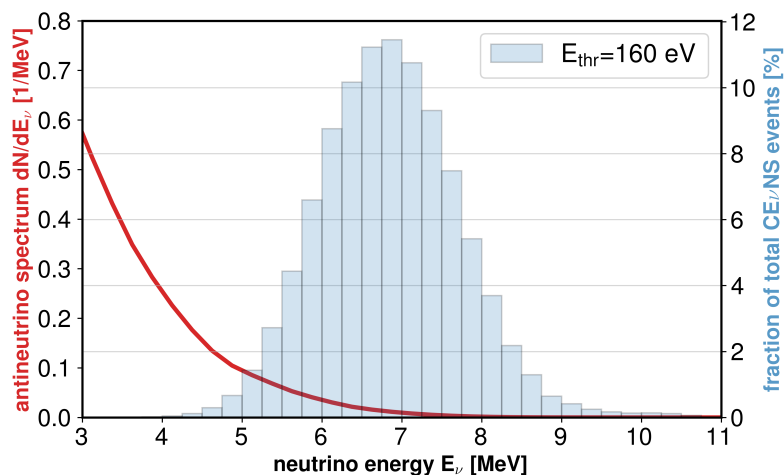


Fig. 9: The fractional contribution of different energy bins in the antineutrino spectrum to the predicted CONUS+ signal events is shown for a threshold of 160 eV_{ee} . The red line indicates the antineutrino spectrum above 3 MeV as emitted from the reactor.

The fractional contribution from antineutrinos of different energies to the signal expectation is quantified in figure 9. At the current detector threshold, we are sensitive to antineutrino energies above 5 MeV. With lower detection threshold, the steep rise in the antineutrino flux towards low energies will result in significantly higher signal expectations [28].